



Spin-orbital nature of the high-field magnetic state in the Sr₄Ru₃O₁₀

Veronica Granata, Lucia Capogna, Filomena Forte, Marie-Bernadette Lepetit,
Rosalba Fittipaldi, Anne Stunault, Mario Cuoco, Antonio Vecchione

► To cite this version:

Veronica Granata, Lucia Capogna, Filomena Forte, Marie-Bernadette Lepetit, Rosalba Fittipaldi, et al.. Spin-orbital nature of the high-field magnetic state in the Sr₄Ru₃O₁₀. Physical Review B, 2016, 93 (11), pp.115128. 10.1103/PhysRevB.93.115128 . hal-01955711

HAL Id: hal-01955711

<https://hal.science/hal-01955711>

Submitted on 25 Feb 2021

HAL is a multi-disciplinary open access archive for the deposit and dissemination of scientific research documents, whether they are published or not. The documents may come from teaching and research institutions in France or abroad, or from public or private research centers.

L'archive ouverte pluridisciplinaire **HAL**, est destinée au dépôt et à la diffusion de documents scientifiques de niveau recherche, publiés ou non, émanant des établissements d'enseignement et de recherche français ou étrangers, des laboratoires publics ou privés.

Spin-orbital nature of the high-field magnetic state in the $\text{Sr}_4\text{Ru}_3\text{O}_{10}$

Veronica Granata,¹ Lucia Capogna,² Filomena Forte,¹ Marie-Bernadette Lepetit,^{3,4} Rosalba Fittipaldi,¹ Anne Stunault,⁴ Mario Cuoco,¹ and Antonio Vecchione¹

¹Consiglio Nazionale delle Ricerche, SPIN, I-84084 Fisciano, and Dipartimento di Fisica “E. R. Caianiello,” Università degli Studi di Salerno, Via G. Paolo II, 132 I-84084 Fisciano, Italy

²Consiglio Nazionale delle Ricerche, IOM OGG, 6 rue J. Horowitz, F-38042 Grenoble, France

³Institut Néel, Centre National de la Recherche Scientifique, UPR 2940, 25 rue des Martyrs, BP 166, F-38042 Grenoble, France

⁴Institut Laue Langevin, 71 Avenue des Martyrs, CS 20156, F-38042 Grenoble Cedex 9, France

(Received 13 August 2015; revised manuscript received 23 February 2016; published 17 March 2016)

We perform a spin-polarized neutron-diffraction study to investigate the nature of the high-field magnetic state of the trilayered $\text{Sr}_4\text{Ru}_3\text{O}_{10}$. The analysis indicates that a high field applied within the ab plane leads to an unbalance of the spin and orbital moments with a spatial profile that is strongly tied to the layers where the electrons are located in the unit cell. We provide evidence of a layer dependent magnetic anisotropy with the inner layers having larger spin and orbital magnetic moments than the outer ones and show that such behavior is robust to temperature variation being persistent above the Curie temperature. By means of an effective model that includes the coupling between the spin-orbital degrees of freedom at inequivalent Ru sites we ascribe the origin of the layer anisotropy to the cooperative effects between octahedral distortions, spin orbit, and Coulomb interactions.

DOI: 10.1103/PhysRevB.93.115128

I. INTRODUCTION

There is consolidated evidence that transition-metal oxides (TMOs) represent an extremely rich source of new phenomena and quantum phases of matter with a high potential for the development of innovative technologies. The competition of different and complex types of order is typical of TMOs mainly due to the strong entanglement and the frustrated localized-itinerant nature of the charge, spin, and orbital degrees of freedom. Though first thought of as a prerogative of $3d$ based TMOs [1,2], this class of phenomena seems now to be ubiquitous in $4d$ and $5d$ systems [3,4] where octahedral distortions, spin-orbit coupling (SOC), and other magnetocrystalline effects often cooperate to yield novel ordered states and proximity to metal-insulator transition, or even Mott insulating states.

A fascinating example of TMOs is the family of ruthenium perovskites belonging to the Ruddlesden-Popper (RP) series $\text{A}_{n+1}\text{Ru}_n\text{O}_{3n+1}$. The ruthenium based RP represents an astonishing natural success to engineer layered materials that can change drastically their electronic and magnetic properties as a function of the number n of RuO_2 layers within the unit cell [5], as well as by rare-earth substitution for alkaline-earth ions or by partial substitution of inequivalent TM ions [6–9]. As a result, the $\text{Sr}_{n+1}\text{Ru}_n\text{O}_{3n+1}$ are metallic and tend to be ferromagnetic (FM) or metamagnetic [10–18], with the exception of the $n = 1$ member that is a spin-triplet superconductor [19,20]. In contrast, the isoelectronic $\text{Ca}_{n+1}\text{Ru}_n\text{O}_{3n+1}$ systems tend to be in proximity to a metal-insulator transition exhibiting antiferromagnetism and rather rich orbital physics [21–30]. Doping Sr onto the Ca sites leads to insulator-to-metal transition accompanied by a changeover from antiferromagnetic to ferromagnetic dominated spin correlations and the occurrence of static magnetic order over nearly the entire range of (Ca,Sr) substitution [31]. To confirm the wide complexity of the phase diagram, novel spin-orbital correlated phenomena [32,33] can be induced by a tiny partial substitution of inequivalent TM

ions in the (Sr,Ca)-RP family as observed, for instance, when Ru ions are replaced by Mn [34–40], Ti [41], Cr [42–47], Fe [48], or other transition-metal elements.

One of the major characteristics of the RP materials is that the physical properties can be critically linked to the number of layers in the unit cell and, hence, to the dimensionality of the electronic environment. Another common aspect is that, for RP members with n different from one, there is a natural emergence of a *layer degree of freedom* which can label the states where the electrons are located in the unit cell. Such an internal degree of freedom, in analogy with electron spin, can be exploited as a carrier of classical or quantum information and thus it may be a relevant ingredient to explore novel electronic device directions, as for instance already proposed in graphene bilayers [49,50] and metal dichalcogenide bilayers [51]. In this context, trilayered perovskites represent a quite unique system with inequivalent layer components when considering the possible mismatch of the inner and outer layers in the unit cell (see Fig. 1). Hence, the fundamental complexity of the RP ruthenates and the potential interrelation to a layer dependent physics makes $\text{Sr}_4\text{Ru}_3\text{O}_{10}$ an intriguing representative case in the family of the triple layered oxides. $\text{Sr}_4\text{Ru}_3\text{O}_{10}$ is an itinerant magnet marked by a strong anisotropy with coexistence of ferromagnetism and metamagnetism. Despite several investigations of the electronic and magnetic properties on this system, there are still unsolved questions both on the microscopic mechanisms that lead to the ferro-meta-magnetic state and on the nature of the resulting phase diagram. There are three key observations that set the $\text{Sr}_4\text{Ru}_3\text{O}_{10}$ magnetic response [14,52]: (i) a ferromagnetic transition occurs at $T_{\text{Curie}} \sim 105$ K, (ii) a magnetic enhancement of the susceptibility occurs at $T^* \sim 60$ K and zero field, and (iii) a metamagnetic transition (i.e., a sharp rising of the magnetization) occurs at $T < T^*$ and for fields applied within the ab plane ($H \parallel ab$) above ~ 2 T. A series of observations contributed to unveil various puzzling features of the metamagnetic phenomena in $\text{Sr}_4\text{Ru}_3\text{O}_{10}$. Transport

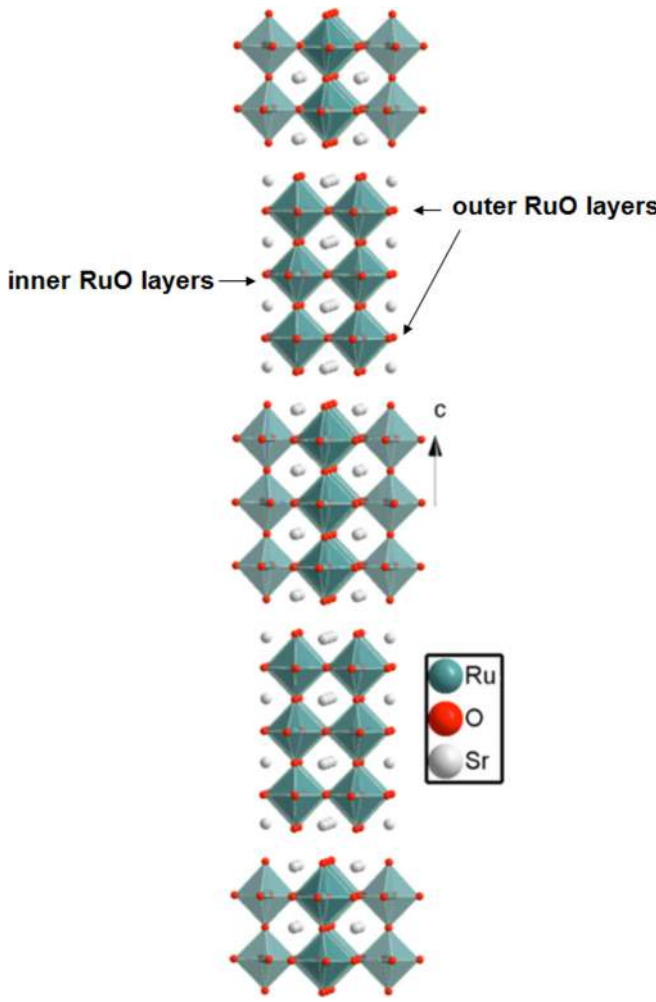


FIG. 1. Schematic of the crystal structure of $\text{Sr}_4\text{Ru}_3\text{O}_{10}$ showing the outer and inner RuO layers in the unit cells along the c axis.

properties showed that the metamagnetic transition lines split as a consequence of a significant spin-orbital coupling [53]. The subtle role of the multiorbital character of the $\text{Sr}_4\text{Ru}_3\text{O}_{10}$ has been also associated to the occurrence of a double metamagnetic transition in high-quality crystals [54]. Furthermore, close to the metamagnetic transition magnetic domains and electronic phase separation can occur [16,55]. Another important ingredient emerging in the $\text{Sr}_4\text{Ru}_3\text{O}_{10}$ metamagnetism is provided by the magnetoelastic coupling [56–59]. In particular, a direct evidence of a strong spin-lattice interaction has been obtained by means of neutron scattering demonstrating how significant structural changes occur concomitantly with the metamagnetic transition [57]. The focus of this work is on the nature of the high-field magnetic state of the $\text{Sr}_4\text{Ru}_3\text{O}_{10}$. We employ polarized neutron scattering to analyze the spin and orbital spatial components of the induced magnetization density $\mathbf{M}(\mathbf{r})$ at high in-plane magnetic fields above the metamagnetic transition. The analysis indicates that the order relation between spin and orbital moments and their amplitudes in the unit cell are strongly tied to the layers where the electrons are located. We find evidence of a layer dependent magnetic anisotropy with the inner layers having larger spin and orbital magnetic moments than the outer ones in the unit

cell. Remarkably, the inner-outer correspondence is robust with respect to temperature variations, being persistent even above T_{Curie} in the paramagnetic state, thus indicating that these features are intrinsic to the high-field magnetic state. In order to investigate the origin of the layer dependent magnetic response, we consider an effective model that describes the coupling between spin and orbital degrees of freedom at different Ru sites in the unit cell. We show that the spin-orbital character of the magnetization in the high field can be ascribed to cooperative effects between octahedral distortions, spin orbit, and Coulomb interactions. The paper is organized as follows. In Sec. II, we introduce the experimental setup and the polarized beam approach. In Sec. III, we present the experimental results, while Sec. IV is devoted to their interpretation and discussion via the effective model. In Sec. V, we provide the concluding remarks.

II. EXPERIMENTAL DETAILS

Single crystals of $\text{Sr}_4\text{Ru}_3\text{O}_{10}$ were grown in an image furnace [60]. The samples were cut into small rectangular slices with an average size of $5 \times 5 \times 0.2 \text{ mm}^3$. Similar samples were already used in previous studies [57]. A number of techniques including x-ray diffraction, energy and wavelength dispersive spectroscopy, as well as neutron Laue diffraction have been employed to fully characterize the structure, the quality, and the purity of the crystals. Magnetization measurements on crystals from the same batch identified the ferromagnetic transition at $T_c \cong 105 \text{ K}$ and a metamagnetic transition at a field of about 2 T when the temperature is lower than $T^* \cong 50 \text{ K}$ and the magnetic field is applied in the ab plane.

Polarized beam measurements were performed on the D3 diffractometer at the Institute Laue Langevin in Grenoble. In such an experiment one measures the flipping ratio R , defined as the ratio of the intensities with neutron polarization parallel and antiparallel to the applied magnetic field. Neglecting corrections such as extinction, half-wavelength contamination, and attenuation, the flipping ratio can be written as [61–63]

$$R = \frac{|F_N(\mathbf{K}) - (\frac{\gamma r_0}{2\mu_B}) 2p F_N(\mathbf{K}) M_\perp(\mathbf{K}) + (\frac{\gamma r_0}{2\mu_B})^2 M_\perp(\mathbf{K})^2|}{|F_N(\mathbf{K}) + (\frac{\gamma r_0}{2\mu_B}) 2p F_N(\mathbf{K}) M_\perp(\mathbf{K}) + (\frac{\gamma r_0}{2\mu_B})^2 M_\perp(\mathbf{K})^2|} \quad (1)$$

where $\gamma r_0 = 5.36 \times 10^{-15} \text{ m}$, and $F_N(\mathbf{K})$ and $M(\mathbf{K})$ are the nuclear structure factor and the Fourier transform of the magnetization density at the scattering vector \mathbf{K} , respectively. $M_\perp(\mathbf{K})$ is the component of $M(\mathbf{K})$ perpendicular to the scattering plane, and p is the incident neutron beam polarization. We observe that at the lowest order of approximation, for small magnetic moments, $R - 1$ is proportional to $M_\perp(\mathbf{K})$.

The data were collected with an incident wavelength $\lambda = 0.825(5) \text{ \AA}$ and polarization $p = 0.95(1)$ and with a 0.5-mm erbium filter in order to reduce higher-order contamination in the incident beam. A Heussler monochromator was used.

The crystal was oriented with the $[hh0/00l]$ plane in the scattering plane. An external magnetic field of 9 T was applied in the $[h\bar{h}0]$ direction prior to cooling and then kept all along while a set of Bragg reflections was measured at 2, 65, and 115 K, which allows us to explore the magnetic

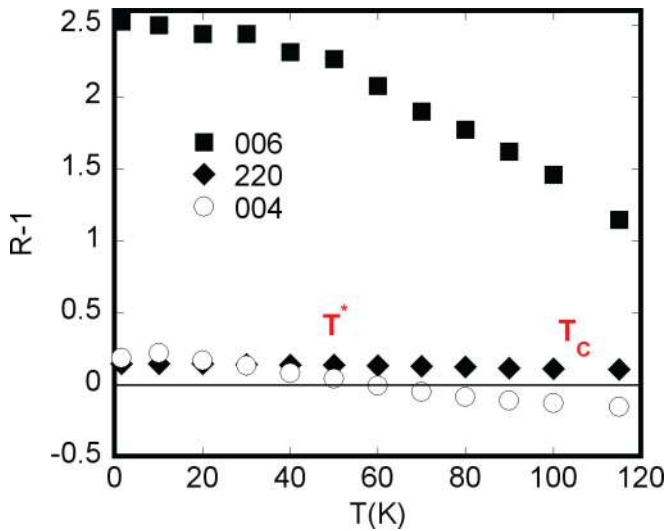


FIG. 2. Temperature dependence of the flipping ratio R , diminished by one, of a few significant Bragg reflections in $\text{Sr}_4\text{Ru}_3\text{O}_{10}$.

configuration within the metamagnetic state, above the metamagnetic transition T^* and the Curie temperature, respectively. At each temperature, we measured over 100 Bragg reflections (corresponding to 37 inequivalent reflections) in the spin-up and spin-down configurations by exploiting the optimization technique as described in Ref. [64]. Finally, the software program Sorgam [65] has been used to determine the magnetic form factors from the measured flipping ratios R .

III. RESULTS

In this section we present the main outcome of the polarized neutron-diffraction measurements and the resulting magnetization profile within the unit cell. Figure 2 shows the temperature dependence of the shifted flipping ratio $R - 1$ at three significant Bragg reflections.

The $R - 1$ for the $(0\ 0\ 6)$ and the $(2\ 2\ 0)$ peaks are positive over the whole range of investigated temperatures. On the other hand, for reflection $(0\ 0\ 4)$, $R - 1$ undergoes a change of sign when the temperature is raised above $T \sim 60$ K.

Assuming that the external magnetic field totally aligns the magnetic moments along the applied direction $[h\bar{h}0]$, one can show that for reflections of the kind $00l$, with even l , the magnetic structure factor $\mathbf{M}_\perp(\mathbf{K})$ in Eq. (1) reduces to

$$\mathbf{M}(00l) = 4\mathbf{m}_c + 16\mathbf{m}_e \cos[\pi l(z_2 + z_3)] \cos[\pi l(z_2 - z_3)]. \quad (2)$$

Here, z_2 and z_3 are the fractional coordinates along the c axis of the two inequivalent ruthenium in the external octahedra of the triple layer.

For $l = 6$, the two terms contributing to the intensity of $\mathbf{M}(\mathbf{K})$, i.e., the one from the central octahedra \mathbf{m}_c and the one from the external ones \mathbf{m}_e , are in phase and therefore add up, whichever the value of the two single terms. In contrast, for $l = 4$, the two terms are in antiphase. As a consequence, for the $(0\ 0\ 4)$ reflection $R - 1$ may change sign, which is indeed observed close to $T \sim 60$ K, suggesting a temperature-dependent transfer of the magnetization from one site to the other in the unit cell. In the case of the $(2\ 2\ 0)$ reflection, all

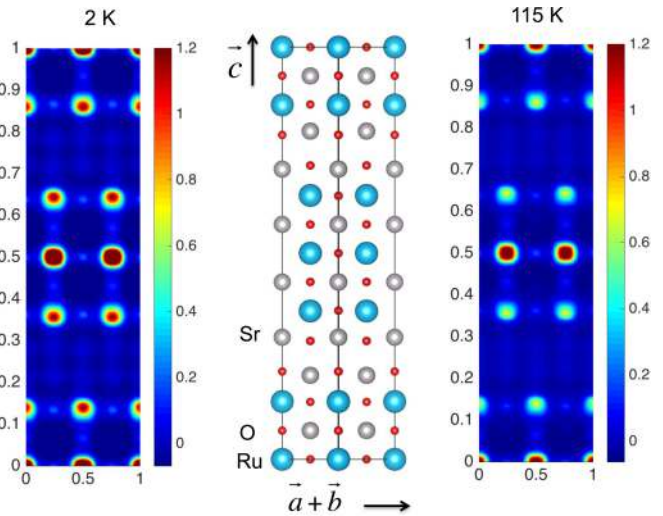


FIG. 3. Spin densities projected onto the $(a + b, c)$ plane, at 2 K (left panel) and 115 K (right panel). Both densities are represented on the same scale, confirming the higher magnetization at low temperature. The middle panel shows the projection of the structure onto the same plane.

the moments contribute in phase to $\mathbf{M}(\mathbf{K})$ and cannot undergo any cancellation due to interference.

In order to give a quantitative picture of such redistribution of spectral weight, we have determined the spatial dependence of the magnetic density below and above the temperature where $R - 1$ changes its sign. Figure 3 shows the spatial contour plot of the spin density within the RuO layers in the unit cell at two representative temperatures, i.e., $T = 2$ and 115 K. The spin densities were obtained from the measured magnetic structure factors by maximum entropy reconstruction [66]. At both temperatures, a set of 37 independent structure factors was used. Figure 3 reports the projections onto the $(a + b, c)$ plane, which was perpendicular to the applied magnetic field. As expected, the main densities are concentrated on the Ru sites, while weaker densities are observed on the oxygen sites. A clear unbalance between the Ru sites also appears clearly in the maps, the densities on the inner Ru ions being higher than those of the outer Ru sites. We do notice that the unbalance is slightly more pronounced in the low-temperature regime.

The magnetic moments for the different ions were refined by means of the program Fullprof [67]. The structural and extinction parameters, obtained from the data collected at the D10 diffractometer of the Institute Laue Langevin, Grenoble, were not varied in the flipping ratio refinement.

For the magnetization density, we have adopted the dipole approximation with the magnetic form factor being only dependent on the magnitude of the scattering vector (spherical distribution):

$$f\left(\frac{|\mathbf{K}|}{2}\right) = \sum_{l=0,2,4,6} W_l \left\langle J_l\left(\frac{|\mathbf{K}|}{2}\right)\right\rangle. \quad (3)$$

Here, $\langle J_l(\frac{|\mathbf{K}|}{2}) \rangle$ are spherical Bessel functions of order l , tabulated in the form of approximations inside Fullprof [68], and W_l are the refinable parameters. Since no radial functions are available for the valence state +4, we have used those of

TABLE I. Refined magnetic moment at three different temperatures for the ruthenium and oxygen atoms. Ru_{1,4} refer to the inner RuO layers, while Ru_{2,3} are in the outer ones (see Fig. 1). A magnetic moment was also allowed on the oxygen ions. Both the total and orbital components are presented. O_a and O_b refer to the apical and basal oxygen sites.

T (K)	2	65	115			
M(μ_B)	M _{tot}	M _{orb}	M _{tot}	M _{orb}	M _{tot}	M _{orb}
Ru _{1,4}	1.52(1)	0.38(8)	1.39(2)	0.320(9)	1.05(2)	0.42(7)
Ru _{2,3}	0.88(1)	0.23(6)	0.74(1)	0.22(6)	0.47(1)	0.11(5)
O _b	0.10(1)		0.08(1)		0.07(5)	
O _a	0.14(1)		0.13(1)		0.09(1)	
χ^2	8.509		4.725		3.398	

the ion Ru⁺¹, which have been already shown to be a good approximation in analogous observations [69].

In the refinement we retain the first two terms, i.e., the ones with coefficients W_0 and W_2 which correspond to the total and the orbital component of the magnetic moments, respectively. In 3d transition-metal systems, the strong crystal-field (CF) interaction dominates over the spin-orbit interaction and the orbital moment is typically quenched. For the layered ruthenates with 4d electrons the spin-orbit coupling is expected to be not negligible and in turn it results in a nontrivial orbital contribution to the total magnetization.

Due to the large unit cell, the refinement procedure has been performed by reducing the number of inequivalent ions contributing to the neutron response. The twelve ruthenium atoms sit in four different crystallographic sites that we indicate as Ru₁, Ru₂, Ru₃, and Ru₄. In order to reduce the free parameters, we sort them into two types: the ruthenium atoms in the central octahedra of the unit cell (Ru₁ and Ru₄) and those in the external octahedra (Ru₂ and Ru₃). As we shall show below, this is physically plausible and consistent with the observed response. Indeed, since the Ru₁ and Ru₄ have similar surrounding anions, their magnetic moments can also be constrained to have the same amplitude, and the same would hold for the Ru₂ and Ru₃.

Furthermore, a magnetic moment was also allowed to occur at the oxygen ions in the RuO₆ octahedra. The presence of unpaired electron density on O_b (the basal ligands) and on O_a (the apical ligands) is found to be quite high. Unlike the case in the compound Ca_{1.5}Sr_{0.5}RuO₄ [70], we observe a sizable moment not only on the basal oxygens but also on the apical ones.

Given the number and the multiplicity of the oxygen sites, we conclude that a significant fraction of magnetization density in the unit cell is transferred from the ruthenium atoms to the oxygens. This is not surprising as the large bandwidth of the Ru-4d orbitals [5,71] close to the Fermi level allows for a significant overlap with the oxygen 2p bands that is typically larger than that in the 3d oxides.

In Table I we present a summary of the magnetic configurations on the inequivalent Ru and O sites for the three investigated temperatures. The amplitude of the orbital

contribution μ_L is significant if compared to the total moment on both types of Ru sites. More specifically, the contribution of the inner layer is found to be larger with respect to the outer, and it is robust to the temperature increase. We observe that, approximately within the estimated errors, the orbital moments of the inner Ru ions as well as the oxygen moments do not vary with temperature. We have tested the statistical fit by imposing constant values as a function of temperature for both the orbital ruthenium moments and the oxygen ones. We point out that the resulting chi square turns out to be slightly greater than that obtained by keeping all the parameters unconstrained.

As far as the total magnetic density is concerned, we can state that a significant layer dependent magnetic anisotropy takes place, which traces back to the unbalance between the larger central and weaker outer components, both in the spin and orbital channels. Moreover, the percentage variation between the two clearly indicates that, by lowering the temperature, part of the magnetization is transferred from the ruthenium in the inner octahedra to those in the outer ones.

IV. EFFECTIVE MODEL AND DISCUSSION

In this section we discuss the microscopic ingredients and the physical mechanisms which are relevant to understand the spin and orbital magnetic response of Sr₄Ru₃O₁₀. Then, we introduce and solve an effective model to present the specific magnetic density configuration that can be obtained in the high-field magnetic state and discuss the connection with the experimental outcome.

A. Mechanism for inequivalent spin-orbital response at the Ru sites

As shown in the previous sections, spin-polarized neutron diffraction provides direct evidence of a sizable orbital component and a net unbalancing of the total magnetic density, both in the orbital and spin sector, between Ru ions belonging to the central and the outer planes of the unit cell.

There are various degrees of freedom to take into account for analyzing the magnetic response. The first important microscopic ingredient is provided by the different octahedral configurations for the surrounding ions of the Ru sites belonging to the inner and the outer layers of the unit cell. Indeed, the octahedral distortions can affect in a distinct way the crystal field potential experienced by the Ru-t_{2g}⁴ electrons close to the Fermi level. In the case of tetrahedral distortions of the RuO₆ octahedra, an inverted hierarchy of the d_{xy} and d_{xz,yz} levels occurs depending on the flat or elongated nature of the deformation and, accordingly, a tendency to a positive or negative orbital polarization $p = n_{xy} - \frac{1}{2}(n_{xz} + n_{yz})$ can be obtained (see Fig. 4). Apart from the structural feature, the breaking of the orbital rotation symmetry due the CF splitting together with a sizable spin-orbit coupling, expected to be relevant in 4d systems, are the other basic elements to be added to properly describe how the variation of the local spin and orbital moments can set the magnetic response [72].

Based on these considerations, we propose and analyze a possible scenario where the magnetic response of each Ru site

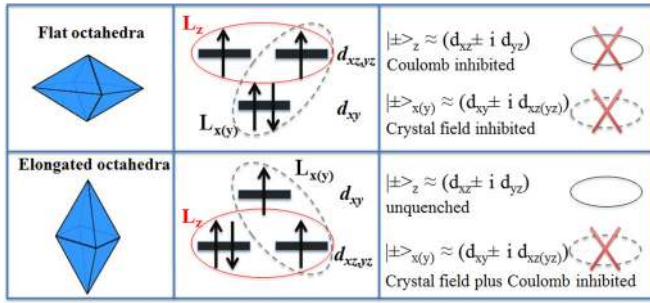


FIG. 4. Schematic representation of the mechanisms which activate/suppress the orbital angular momentum components in the absence of an in-plane applied magnetic field, in the case of a flat octahedron (upper panel) and an elongated octahedron (lower panel). Middle panels show representative local configurations that mark the ground state. Right panels describe the orbital polarized configurations that are favored or inhibited with respect to the crystal-field potential and the Coulomb interaction.

in the inner and outer layers crucially depends on the specific character of the tetrahedral deformations, i.e., the degree of flattening/elongation, and its competition with local Coulomb interaction and spin-orbit coupling.

The mechanism for having an inequivalent magnetic response at different Ru sites is illustrated by the sketch in Fig. 4. The key observation is that the local configurations at the Ru sites, as shown in the middle panels of Fig. 4, can have an orbital polarization for which the competition between the Coulomb interaction and the spin-orbit coupling in the presence of the crystal-field potential can be significantly different. We first consider the case of flat octahedra, which is reported in the upper panels of Fig. 4. In this case the local configurations at the Ru site, which is representative of the ground state with four electrons in the t_{2g} sector (i.e., Ru-4d⁴), can have a preferential occupation of the d_{xy} orbital as due to the CF potential. In the absence of any applied magnetic field, the in-plane $L_{x,y}$ components of the orbital angular momentum \mathbf{L} and the corresponding SOC activated terms ($L_x S_x + L_y S_y$) are mainly inhibited by the CF splitting. On the other hand, the out-of-plane L_z and the related $L_z S_z$ term of the SOC can be equally hindered by the Coulomb interaction that tends to favor a fully aligned spin-triplet state. Hence, in the regime where all these energy scales are of the same order of magnitude and thus compete, the response to an applied field is expected to be mainly isotropic, in both the orbital and spin channels.

In the elongated case (lower panel of Fig. 4), the hierarchy of the t_{2g} orbitals is different and the minority spin prefers to occupy the $d_{xz,yz}$ sector. While the $L_{x,y}$ can be still inhibited by the CF, the L_z and the relative SOC term $L_z S_z$ are now unaffected by the local Coulomb interaction. The result is that there is an emergence of a local *easy* polarization axis both for the spin and the orbital components, which can lead to an anisotropic response to an applied field in the case of Ru sites belonging to elongated octahedra. Then, we are brought to deduce that the in-plane magnetic moments would be harder to be polarized at the Ru sites having elongated octahedra since in this case the applied field is orthogonal to the easy orbital axis z . On the contrary, there will be a greater susceptibility to an in-plane magnetic field at the Ru sites with flat octahedra,

as in this case the magnetic isotropy makes the moments more easily oriented.

B. Model

In order to quantitatively support the physical scenario introduced above, we consider a model Hamiltonian with two inequivalent Ru atoms that includes all the local interactions of the electrons in the t_{2g} sector and allows for an effective charge transfer between them.

The inequivalent Ru sites are indicated with Ru_{fl} and Ru_{el} to label the compressive and the elongated distortions of the corresponding octahedra. The Hamiltonian H for the correlated electron in the t_{2g} manifold is expressed as a sum of different contributions:

$$H = H_{\text{kin}} + H_{\text{el-el}} + H_{\text{CF}} + H_{\text{SO}} + H_{x,y}. \quad (4)$$

The first term in Eq. (4) is the kinetic contribution between the t_{2g} orbitals on different Ru sites, $H_{\text{el-el}}$ is the local Coulomb interaction expressed in term of the couplings U and J_H , H_{CF} stands for the crystalline-field potential via the parameter Δ , H_{SO} indicates the spin-orbit term through the coupling λ , and $H_{x,y}$ describes the in-plane applied Zeeman field B (see the Appendix for details).

The complete Hamiltonian embodies five interaction parameters. We follow local-density approximation predictions [5] and assign, in the calculations, the values $t = 0.4$ eV and $\Delta_{fl}/t = -0.3, \Delta_{el}/t = 0.225$ to the CF parameters of the central-flat and outer-elongated octahedra, respectively. In the second instance, we will also vary the CF parameters, in order to simulate possible magnetoelastic effects driven by the applied field. Concerning the Coulomb interactions, we consider the ratio $U/J_H = 5.0$ and analyze the regime of intermediate electronic correlations set by $U/t = 5.0$ [73]. We also include the SOC term the amplitude of which is $\lambda/t = 0.14$, in the range of values that is expected to hold for Sr-based ruthenates [74]. It is worth pointing out that the interplay of the Coulomb and spin-orbit interactions has an important role in determining the magnetic responses. Indeed, a choice of a different regime of amplitudes for U and λ would significantly modify the local configurations contributing to the ground state and in turn alter the resulting spin and orbital response.

C. Ground-state properties: Zeeman field response and role of distortions

In this subsection, we analyze the ground-state properties by solving the model Hamiltonian in Eq. (4) by exact diagonalization in a physical regime that is relevant for the $Sr_4Ru_3O_{10}$ compound.

In Figs. 5(a1) and 5(a2) we present the field dependence of the local in-plane orbital m_L and spin m_S components of the total magnetic density at the flat and elongated Ru sites, upon the application of an in-plane Zeeman field. As one can notice, the magnetic response is dominated by configurations where the spin moment is larger than the orbital one (in absolute value) and the spin-orbital moments at the flat Ru sites overcome those associated with the elongated octahedra. The evolution of the magnetic moments is marked by two

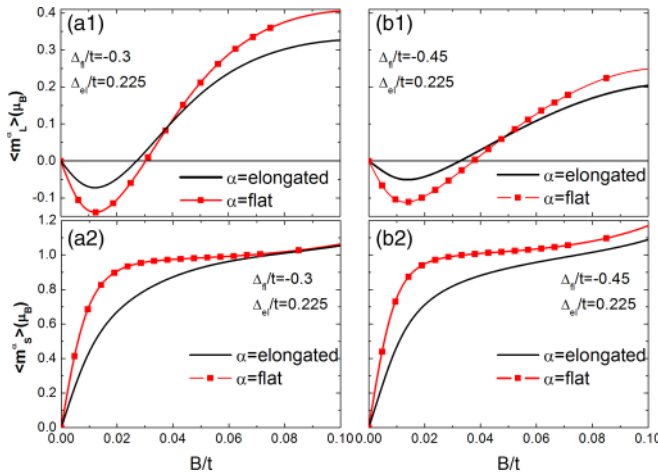


FIG. 5. Evolution of the orbital (a1 and b1) and spin (a2 and b2) components of the magnetic density upon an in-plane applied Zeeman field, for two different values of the compressive crystal-field potential, i.e., (a) $\Delta_{fi}/t = -0.3$ and (b) $\Delta_{fi}/t = -0.45$.

different regimes. In the low-field region $B/t \lesssim 0.03$, m_L and m_S have opposite signs, while they are parallel oriented above this threshold. This behavior is expected due to the spin-orbit coupling that tends to form a local $J = 0$ singlet with $J = L + S$ and thus contributes to have the spin and the orbital angular moments in an antialigned orientation within the ground state. The spin magnetic moment m_S grows linearly with the field and promptly exhibits a larger contribution of Ru_{fl} . These features are easily reconciled within the scheme depicted in Fig. 4. Indeed, for elongated octahedra, the existence of the easy orbital axis z makes the spin-orbital response at low fields quite stiff. In contrast, in the flat case, there is no privileged quantization axis and both the in-plane spin and angular magnetic moments have a comparable response to the applied field. We point out that, in this window of parameters, the spin and orbital moment are not fully polarized as expected when the field is much smaller than the other involved energy scales. The amplitude of the spin magnetic moment reaches the value $1\mu_B$ while for the orbital part one gets $0.4\mu_B$ and $0.3\mu_B$, respectively.

Next, we consider the possibility to tune the CF strength to mimic an effective magnetoelastic coupling or a physical situation where a structural change occurs with the application of a magnetic field.

In the regime of high magnetic fields, there are no available *ab initio* data or complete information on the unit-cell atomic positions, and thus the theoretical estimates of the CF parameters are lacking. We also notice that it is not possible to extract any indirect estimate of the CF parameters from the performed neutron measurements, since they were collected in an experimental configuration which was optimized to study the magnetic structure and not aimed at determining the nuclear structure. Hence, we referred to recent neutron-scattering experiments [57], demonstrating that a significant shrinking of the unit cell along the c axis occurs concomitantly with the metamagnetic transition. On the basis of this experimental observation, we infer that the reduction of the c -axis parameter should naturally lead to an

overall compression of the apical Ru-O distances. Due to the symmetry between the two Ru sites forming the cluster under examination, the variation of the Ru-O apical bond length can be simulated by an increased CF potential for the Ru site of the flat octahedral only, without loss of generality. Hence, we have selected the regime in which the crystal-field potential for the Ru site of the flat octahedra increases. In Figs. 5(b1) and 5(b2) we report the evolution of the orbital and spin contributions to the magnetic density in the case of a more pronounced compressive potential, i.e., $\Delta_{fl}/t = -0.45$, while Δ_{el} is kept unchanged. The increased value of Δ_{fl}/t modifies the behavior of the response both at low and high fields. In particular, the orbital moment shows a reduction of both the flat and elongated components, with a major percentage reduction of the former which indeed is hindered by the crystal-field potential (see Fig. 4). In contrast, the slope of the spin curve for flat octahedra shows an appreciable upturn, which is indicative of a stronger spin susceptibility. Interestingly, at high fields there is an increase of the spin unbalance between the magnetic moments at the two Ru sites indicating that the relation between the spin response and the octahedral deformation can be highly nontrivial particularly concerning the amplitude of the effects. Furthermore, the specific relation between spin and orbital moments at the two inequivalent Ru sites is strongly dependent on the strength of the spin-orbit and Coulomb interactions. A decrease of these interactions will affect both qualitatively and quantitatively the response to an applied field.

D. Temperature dependence of the spin and orbital magnetic moments

To conclude this section, we present the thermal evolution of the spin and orbital densities as a function of the microscopic parameters involved in the model, by mainly focusing on the regime of moderate-to-strong Coulomb correlations, intermediate spin-orbit coupling, and high magnetic fields, where the theoretical outcomes at $T = 0$ exhibit the best agreement with the low-temperature experiments. The comparison is made both on the absolute amplitude of the spin-orbital moments and the degree of unbalancing between the flat and elongated layers. The study performed at finite temperature strengthens and, at the same time, enriches the scenario we propose by revealing interesting features of the layer dependent magnetic anisotropy. One of the main findings is that this effect is stable over a wide range of temperatures. On a general ground the spin and orbital densities exhibit a small amplitude change by raising the temperature. Nevertheless, we underline a distinct response of the spin and orbital component in the high-temperature regime. Concerning the spin density, the response is generally not much affected both in the flat and elongated cases, though, in a wide range of parameters, it tends to exhibit a maximum and then it gradually decreases, as expected, due to thermal fluctuations. The specific spin response is strongly related to the competing ferro- and antiferromagnetic correlations in the ground state of the small cluster and somehow overestimates the strength of the short-range correlations with a resulting smooth increase at small temperatures. In contrast, the orbital moment appears to be promptly reduced in both channels. Furthermore, the

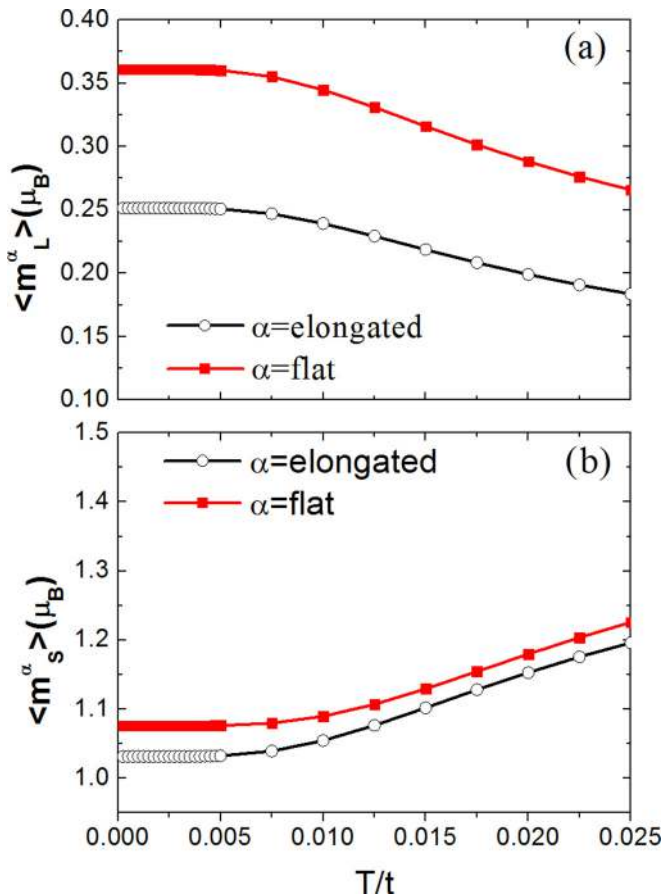


FIG. 6. Thermal evolution of the (a) spin and (b) orbital components of the magnetic density for an in-plane applied Zeeman field $B/t = 0.1$, spin-orbit coupling $\lambda/t = 0.3$, and values of the crystal-field potential given by $\Delta_{fl}/t = -0.45$ and $\Delta_{el}/t = 0.225$.

degree of the anisotropy for the flat and elongated channels stays almost constant upon temperature. Another interesting aspect emerging in the complete scan of the phase space is that, depending on the regime set by the spin-orbit coupling, one can find that the order relation among the total magnetic densities of the two layers is not preserved when thermally ramping up from low to high temperatures (e.g., above room temperature). Indeed, in the moderate-to-strong spin-orbit regime (i.e., $\lambda/t > \lambda_c \approx 0.3$), we have verified the existence of a characteristic temperature \tilde{T} , above which the moments at the elongated Ru sites carry the larger contribution within the unit cell. We have also analyzed the dependence of \tilde{T} upon the microscopic parameters and found that the value of \tilde{T} turns out to be independent of the applied field B , while it is strongly varying with the Coulomb repulsion U and the spin-orbit coupling. In this respect, we point out that this result adds another constraint to the regime of microscopic interactions that can optimally capture the spin-orbital nature of the high-field magnetic state in the three-layered ruthenate perovskite as described within the proposed model.

As a representative case of the thermal dependence of the magnetic anisotropy we report in Fig. 6 the high-field (i.e., $B/t = 0.1$) evolution of the spin and orbital components for an optimal set of parameters, i.e., $\Delta_{fl}/t = -0.45$, $\Delta_{el}/t =$

0.225, $\lambda/t = 0.3$, and keeping the Coulomb interactions unchanged with respect to the zero-temperature results of Fig. 5, i.e., $U/J_H = 5.0$ and $U/t = 5.0$. The spin and orbital densities have a small amplitude change (about 10%) by raising the temperature up to $T/t \sim 0.025$, which covers the experimental range of investigated temperatures (i.e., for $t \sim 400$ meV, T is of the order of 110 K). Such a variation is compatible with the experimental observations and confirms the robustness of the anisotropy with respect to the temperature fluctuations.

V. CONCLUSIONS

In conclusion, by means of polarized neutron-scattering diffraction we have determined the spin and orbital character of the high-field magnetic state of $\text{Sr}_4\text{Ru}_3\text{O}_{10}$. Interestingly, the spin-orbital moment distribution in the high-field state is not much affected by temperature, thus indicating that its origin should not be critically related with the ferromagnetic and the metamagnetic phenomena in $\text{Sr}_4\text{Ru}_3\text{O}_{10}$. We show that the layer degree of freedom can play a role in the magnetic response of the system with a layer dependent magnetic anisotropy marked by the inner layers exhibiting spin and orbital magnetic moments that are larger than the outer ones. We discuss the origin of this layer dependent magnetic anisotropy in terms of inequivalent distorted octahedra, spin-orbit coupling, and local Coulomb correlations. The analysis indicates that local structural changes of the octahedra and spin-orbit cannot account by themselves for the hierarchy between spin and orbital magnetic moments at the inner and outer layers of the unit cell. It is only the cooperative effect between the spin-orbit coupling, the crystal-field potential, and the Coulomb coupling which leads to the unbalance between the spin and orbital moments in the magnetic response at the inequivalent Ru sites. In light of the performed analysis, we argue that the high-field magnetic state for an applied field along the c axis might exhibit an analogous layer dependent magnetic distribution but with an opposite trend between the inner and the outer layers. Such investigation might provide more insight into the fundamental mechanisms that control the ferromagnetic and the metamagnetic behavior in $\text{Sr}_4\text{Ru}_3\text{O}_{10}$. Due to the general ingredients of the discussed mechanism, one can also suggest that similar effects can be observed in other systems where inequivalent local orbital polarizations in the presence of competing spin orbit and Coulomb interaction can lead to distinct spin-orbital responses.

ACKNOWLEDGMENTS

We acknowledge insightful discussions and valuable support during the experiments from Paul Steffens and Laurent Chapon.

APPENDIX

The model Hamiltonian used for the theoretical analysis reads

$$H_{\text{kin}} = -t \sum_{i,j,\sigma} (d_{i\sigma}^\dagger d_{j\sigma} + \text{H.c.}), \quad (\text{A1})$$

$d_{i\alpha\sigma}^\dagger$ being the creation operator for an electron with spin σ at the i site in the α orbital. The hopping amplitude in H_{kin} is assumed to be t for the orbitals in the t_{2g} manifold. The second term is the local Coulomb interaction between t_{2g} electrons:

$$H_{\text{el-el}} = U \sum_{i\alpha} n_{i\alpha\uparrow} n_{i\alpha\downarrow} - 2J_H \sum_{i\alpha\beta} \mathbf{S}_{i\alpha} \cdot \mathbf{S}_{i\beta} + \left(U' - \frac{J_H}{2} \right) \times \sum_{i\alpha\neq\beta} n_{i\alpha} n_{i\beta} + J' \sum_{i\alpha\beta} d_{i\alpha\uparrow}^\dagger d_{i\alpha\downarrow}^\dagger d_{i\beta\uparrow} d_{i\beta\downarrow} \quad (\text{A2})$$

where $n_{i\alpha\sigma}, \mathbf{S}_{i\alpha}$ are the on-site charge for spin σ and the spin operators for the α orbital, respectively. U (U') is the intraorbital (interorbital) Coulomb repulsion, J_H is the Hund coupling, and J' is the pair hopping term. Due to the invariance for rotations in the orbital space, the following relations hold: $U = U' + 2J_H, J' = J_H$.

The H_{CF} part of the Hamiltonian H is the crystalline-field potential, controlling the symmetry lowering from the cubic to tetragonal one:

$$H_{\text{CF}} = \sum_i \Delta_i \left[n_{ixy} - \frac{1}{2} (n_{ixz} + n_{iyz}) \right]. \quad (\text{A3})$$

Positive (negative) values of Δ are related to elongated (flat) RuO_6 octahedron along the c axis and favor the

occupation in the $d_{xz,yz}$ (d_{xy}) sector, respectively. For the present investigation, we consider $\Delta_1 = \Delta_{fl}$ to be positive while $\Delta_2 = \Delta_{el}$ is negative.

Since we deal with $4d$ oxides, it is also important to include the spin-orbit coupling

$$H_{\text{SO}} = \lambda \sum_i \mathbf{L}_i \cdot \mathbf{S}_i \quad (\text{A4})$$

where λ is the spin-orbit coupling constant, \mathbf{L}_i is the total orbital momentum, and \mathbf{S}_i is the total spin of the t_{2g} states.

Finally, $H_{x,y}$ in Eq. (4) describes the Zeeman coupling of the local angular momenta to a magnetic field B applied in the ab plane along the x, y symmetry directions, expressed in units of the Bohr magneton:

$$H_{x,y} = \sum_i (\mathbf{L}_i + 2\mathbf{S}_i) \cdot \mathbf{B}_{x,y}. \quad (\text{A5})$$

Within the presented analysis, we have neglected the in-plane anisotropy and thus x and y directions are assumed to be equivalent. Such a minimal model contains all the relevant couplings between the local spin and orbital degrees through the spin orbit and the Coulomb interaction as well as the possibility for having charge fluctuations in the t_{2g} via the kinetic term that links the two atoms.

-
- [1] M. Imada, A. Fujimori, and Y. Tokura, *Rev. Mod. Phys.* **70**, 1039 (1998).
 - [2] E. Dagotto, *Science* **309**, 257 (2005).
 - [3] B. J. Kim, H. Ohsumi, T. Komesu, S. Sakai, T. Morita, H. Takagi, and T. Arima, *Science* **323**, 1329 (2009).
 - [4] D. Pesin and L. Balents, *Nature Physics* **6**, 376 (2010).
 - [5] M. Malvestuto, E. Carleschi, R. Fittipaldi, E. Gorelov, E. Pavarini, M. Cuoco, Y. Maeno, F. Parmigiani, and A. Vecchione, *Phys. Rev. B* **83**, 165121 (2011).
 - [6] T. F. Qi, O. B. Korneta, L. Li, K. Butrouna, V. S. Cao, Xiangang Wan, P. Schlottmann, R. K. Kaul, and G. Cao, *Phys. Rev. B* **86**, 125105 (2012).
 - [7] Y. Cao *et al.*, [arXiv:1406.4978](#).
 - [8] H. Lei, W.-G. Yin, Z. Zhong, and H. Hosono, *Phys. Rev. B* **89**, 020409(R) (2014).
 - [9] C. Dhital *et al.*, *Nat. Comm.* **5**, 3377 (2014).
 - [10] L. Klein, J. S. Dodge, C. H. Ahn, G. J. Snyder, T. H. Geballe, M. R. Beasley, and A. Kapitulnik, *Phys. Rev. Lett.* **77**, 2774 (1996).
 - [11] P. B. Allen, H. Berger, O. Chauvet, L. Forro, T. Jarlborg, A. Junod, B. Revaz, and G. Santi, *Phys. Rev. B* **53**, 4393 (1996).
 - [12] S. A. Grigera, R. S. Perry, A. J. Schofield, M. Chiao, S. R. Julian, G. G. Lonzarich, S. I. Ikeda, Y. Maeno, A. J. Millis, and A. P. Mackenzie, *Science* **294**, 329 (2001).
 - [13] R. S. Perry, L. M. Galvin, S. A. Grigera, L. Capogna, A. J. Schofield, A. P. Mackenzie, M. Chiao, S. R. Julian, S. I. Ikeda, S. Nakatsuji, Y. Maeno, and C. Pfleiderer, *Phys. Rev. Lett.* **86**, 2661 (2001).
 - [14] G. Cao, L. Balicas, W. H. Song, Y. P. Sun, Y. Xin, V. A. Bondarenko, J. W. Brill, S. Parkin, and X. N. Lin, *Phys. Rev. B* **68**, 174409 (2003).
 - [15] A. G. Green, S. A. Grigera, R. A. Borzi, A. P. Mackenzie, R. S. Perry, and B. D. Simons, *Phys. Rev. Lett.* **95**, 086402 (2005).
 - [16] Z. Q. Mao, M. Zhou, J. Hooper, V. Golub, and C. J. O'Connor, *Phys. Rev. Lett.* **96**, 077205 (2006).
 - [17] D. Fobes, M. H. Yu, M. Zhou, J. Hooper, C. J. O'Connor, M. Rosario, and Z. Q. Mao, *Phys. Rev. B* **75**, 094429 (2007).
 - [18] A. Tamai, M. P. Allan, J. F. Mercure, W. Meevasana, R. Dunkel, D. H. Lu, R. S. Perry, A. P. Mackenzie, D. J. Singh, Z.-X. Shen, and F. Baumberger, *Phys. Rev. Lett.* **101**, 026407 (2008).
 - [19] Y. Maeno, H. Hashimoto, K. Yoshida, S. NishiZaki, T. Fujita, J. G. Bednorz, and F. Lichtenberg, *Nature (London)* **372**, 532 (1994).
 - [20] A. Mackenzie and Y. Maeno, *Rev. Mod. Phys.* **75**, 657 (2003).
 - [21] G. Cao, S. C. McCall, J. E. Crow, and R. P. Guertin, *Phys. Rev. B* **56**, 5387 (1997).
 - [22] H. L. Liu, S. Yoon, S. L. Cooper, G. Cao, and J. E. Crow, *Phys. Rev. B* **60**, R6980 (1999).
 - [23] S. Nakatsuji and Y. Maeno, *Phys. Rev. B* **62**, 6458 (2000).
 - [24] T. Mizokawa, L. H. Tjeng, G. A. Sawatzky, G. Ghiringhelli, O. Tjernberg, N. B. Brookes, H. Fukazawa, S. Nakatsuji, and Y. Maeno, *Phys. Rev. Lett.* **87**, 077202 (2001).
 - [25] F. Nakamura, T. Goko, M. Ito, T. Fujita, S. Nakatsuji, H. Fukazawa, Y. Maeno, P. Alireza, D. Forsythe, and S. R. Julian, *Phys. Rev. B* **65**, 220402 (2002).
 - [26] C. S. Snow, S. L. Cooper, G. Cao, J. E. Crow, H. Fukazawa, S. Nakatsuji, and Y. Maeno, *Phys. Rev. Lett.* **89**, 226401 (2002).
 - [27] J. S. Lee, Y. S. Lee, T. W. Noh, S.-J. Oh, J. Yu, S. Nakatsuji, H. Fukazawa, and Y. Maeno, *Phys. Rev. Lett.* **89**, 257402 (2002).
 - [28] J. H. Jung, Z. Fang, J. P. He, Y. Kaneko, Y. Okimoto, and Y. Tokura, *Phys. Rev. Lett.* **91**, 056403 (2003).

- [29] A. Koga, N. Kawakami, T. M. Rice, and M. Sigrist, *Phys. Rev. Lett.* **92**, 216402 (2004).
- [30] V. I. Anisimov, I. A. Nekrasov, D. E. Kondakov, T. M. Rice, and M. Sigrist, *Eur. Phys. J. B* **25**, 191 (2002).
- [31] J. P. Carlo *et al.*, *Nat. Mater.* **11**, 323 (2012).
- [32] W. Brzezicki, A. M. Oles, and M. Cuoco, *Phys. Rev. X* **5**, 011037 (2015).
- [33] W. Brzezicki, C. Noce, A. Romano, and M. Cuoco, *Phys. Rev. Lett.* **114**, 247002 (2015).
- [34] R. Mathieu, A. Asamitsu, Y. Kaneko, J. P. He, X. Z. Yu, R. Kumai, Y. Onose, N. Takeshita, T. Arima, H. Takagi, and Y. Tokura, *Phys. Rev. B* **72**, 092404 (2005).
- [35] J. E. Ortmann, J. Y. Liu, J. Hu, M. Zhu, J. Peng, M. Matsuda, X. Ke, and Z. Q. Mao, *Scientific Reports* **3**, 2950 (2013).
- [36] B. Hu, G. T. McCandless, V. O. Garlea, S. Stadler, Y. Xiong, J. Y. Chan, E. W. Plummer, and R. Jin, *Phys. Rev. B* **84**, 174411 (2011).
- [37] M. A. Hossain, B. Bohnenbuck, Y. D. Chuang, M. W. Haverkort, I. S. Elfimov, A. Tanaka, A. G. Cruz Gonzalez, Z. Hu, H. J. Lin, C. T. Chen, R. Mathieu, Y. Tokura, Y. Yoshida, L. H. Tjeng, Z. Hussain, B. Keimer, G. A. Sawatzky, and A. Damascelli, *Phys. Rev. B* **86**, 041102(R) (2012).
- [38] G. Panaccione *et al.*, *New Journal of Physics* **13**, 053059 (2011).
- [39] D. Mesa, F. Ye, S. Chi, J. A. Fernandez-Baca, W. Tian, B. Hu, R. Jin, E. W. Plummer, and J. Zhang, *Phys. Rev. B* **85**, 180410(R) (2012).
- [40] G. Li, Q. Li, M. Pan, B. Hu, C. Chen, J. Teng, Z. Diao, J. Zhang, R. Jin, and E. W. Plummer, *Sci. Rep.* **3**, 2882 (2013).
- [41] X. Ke, J. Peng, D. J. Singh, T. Hong, W. Tian, C. R. Dela Cruz, and Z. Q. Mao, *Phys. Rev. B* **84**, 201102(R) (2011).
- [42] Li Pi, A. Maignan, R. Retoux, and B. Raveau, *J. Phys.: Condens. Matter* **14**, 7391 (2002).
- [43] B. Dabrowski, O. Chmaissem, P. W. Klamut, S. Kolesnik, M. Maxwell, J. Mais, Y. Ito, B. D. Armstrong, J. D. Jorgensen, and S. Short, *Phys. Rev. B* **70**, 014423 (2004).
- [44] Z. H. Han, J. I. Budnick, W. A. Hines, B. Dabrowski, S. Kolesnik, and T. Maxwell, *J. Phys.: Condens. Matter* **17**, 1193 (2005).
- [45] V. Durairaj, S. Chikara, X. N. Lin, A. Douglass, G. Cao, P. Schlottmann, E. S. Choi, and R. P. Guertin, *Phys. Rev. B* **73**, 214414 (2006).
- [46] G. Cao, V. Durairaj, S. Chikara, L. E. DeLong, and P. Schlottmann, *Phys. Rev. Lett.* **100**, 016604 (2008).
- [47] T. F. Qi, O. B. Korneta, S. Parkin, L. E. De Long, P. Schlottmann, and G. Cao, *Phys. Rev. Lett.* **105**, 177203 (2010).
- [48] X. Ke, J. Peng, W. Tian, Tao Hong, M. Zhu, and Z. Q. Mao, *Phys. Rev. B* **89**, 220407(R) (2014).
- [49] P. San-Jose, E. Prada, E. McCann, and H. Schomerus, *Phys. Rev. Lett.* **102**, 247204 (2009).
- [50] D. Pesin and A. H. MacDonald, *Nat. Mater.* **11**, 409 (2012).
- [51] Z. Gong, G.-B. Lin, H. Yu, D. Xiao, X. Cui, X. Xu, and W. Yao, *Nat. Comm.* **4**, 2053 (2013).
- [52] M. K. Crawford, R. L. Harlow, W. Marshall, Z. Li, G. Cao, R. L. Lindstrom, Q. Huang, and J. W. Lynn, *Phys. Rev. B* **65**, 214412 (2002).
- [53] Y. J. Jo, L. Balicas, N. Kikugawa, E. S. Choi, K. Storr, M. Zhou, and Z. Q. Mao, *Phys. Rev. B* **75**, 094413 (2007).
- [54] E. Carleschi, B. P. Doyle, R. Fittipaldi, V. Granata, A. M. Strydom, M. Cuoco, and A. Vecchione, *Phys. Rev. B* **90**, 205120 (2014).
- [55] D. Fobes, T. J. Liu, Z. Qu, M. Zhou, J. Hooper, M. Salamon, and Z. Q. Mao, *Phys. Rev. B* **81**, 172402 (2010).
- [56] R. Gupta, M. Kim, H. Barath, S. L. Cooper, and G. Cao, *Phys. Rev. Lett.* **96**, 067004 (2006).
- [57] V. Granata, L. Capogna, M. Reehuis, R. Fittipaldi, B. Ouladdiaf, S. Pace, M. Cuoco, and A. Vecchione, *J. Phys.: Condens. Matter* **25**, 056004 (2013).
- [58] M. Iliev, V. Popov, A. Litvinchuk, M. Abrashev, J. Backstrom, Y. Sun, R. Meng, and C. Chu, *Phys. B (Amsterdam)* **358**, 138 (2005).
- [59] C. Mirri, F. M. Vitucci, P. Di Pietro, S. Lupi, R. Fittipaldi, V. Granata, A. Vecchione, U. Schade, and P. Calvani, *Phys. Rev. B* **85**, 235124 (2012).
- [60] R. Fittipaldi *et al.*, *Crystal Growth and Design* **7**, 2495 (2007).
- [61] G. L. Squires, *Introduction to the Theory of Thermal Neutron Scattering* (Cambridge University, Cambridge, England, 1978).
- [62] R. Nathans, S. J. Pickart, H. Alperin, and P. J. Brown, *Phys. Rev.* **136**, A1641 (1964).
- [63] A. Delapalme, R. Georges, and J. Schweizer, *Nucl. Instr and Methods* **63**, 283 (1968).
- [64] E. Lelievre-Berna *et al.*, *Physica B* **397**, 138 (2007).
- [65] <https://www.ill.eu/sites/ccl/appnx/sorgam.html>.
- [66] *Maximum Entropy and Bayesian Methods*, edited by J. Skilling (Kluwer, Dordrecht, 1989); R. J. Papoular and B. Gillon, *Europhys. Lett.* **13**, 429 (1990); S. F. Gull and J. Skilling, *MEMSYS III Quantified Maximum Entropy Subroutine Library* (Maximum Entropy Data Consultants Ltd. Royston, UK, 1989).
- [67] J. Rodriguez Carvajal, *Physica B* **192**, 55 (1993).
- [68] See International Tables for Crystallography, Vol. C.
- [69] L. Capogna, E. M. Forgan, G. J. McIntyre, N. Burton, P. G. Kealey, R. S. Perry, L. M. Galvin, A. P. Mackenzie, S. Ikeda, and Y. Maeno, *Appl. Phys. A* **74**, S928 (2002).
- [70] A. Gukasov, M. Braden, R. J. Papoular, S. Nakatsuji, and Y. Maeno, *Phys. Rev. Lett.* **89**, 087202 (2002).
- [71] I. I. Mazin and D. J. Singh, *Phys. Rev. Lett.* **79**, 733 (1997).
- [72] M. Cuoco, F. Forte, and C. Noce, *Phys. Rev. B* **73**, 094428 (2006).
- [73] E. Gorelov, M. Karolak, T. O. Wehling, F. Lechermann, A. I. Lichtenstein, and E. Pavarini, *Phys. Rev. Lett.* **104**, 226401 (2010).
- [74] M. W. Haverkort, I. S. Elfimov, L. H. Tjeng, G. A. Sawatzky, and A. Damascelli, *Phys. Rev. Lett.* **101**, 026406 (2008).